Hindawi
Journal of Nanomaterials
Volume 2018, Article ID 5456731, 9 pages
https://doi.org/10.1155/2018/5456731

Research Article

Evaluation of Serum-Paired miRNA Ratios for Early Diagnosis of Non-Small Cell Lung Cancer Using Quantum Dot-Based Suspension Array

Lihong Fan,[1] Hao Chen,[2] Junliang Teng,[3] Dan Li,[4] Changhui Wang,[1] Qing Xia,[1] Bo Su,[5] and Huiwei Qi[6]

[1]*Department of Respiration Medicine, Shanghai Tenth People's Hospital, Tongji University School of Medicine, Shanghai 200072, China*
[2]*Departments of Oncology and Respiration Medicine, Shanghai Tenth People's Hospital, Tongji University School of Medicine, Shanghai 200072, China*
[3]*School of Information Management and Engineering, Shanghai University of Finance and Economics, Shanghai 200433, China*
[4]*Department of Nuclear Medicine, Shanghai Tenth People's Hospital, Tongji University School of Medicine, Shanghai 200072, China*
[5]*Central Laboratory, Shanghai Pulmonary Hospital, Tongji University School of Medicine, Shanghai 200433, China*
[6]*Department of Oncology, Shanghai Pulmonary Hospital, Tongji University School of Medicine, Shanghai 200433, China*

Correspondence should be addressed to Bo Su; su_bo_s@hotmail.com and Huiwei Qi; huiwei_queen@163.com

Received 8 February 2018; Revised 4 May 2018; Accepted 4 June 2018; Published 1 August 2018

Academic Editor: William Yu

Non-small cell lung cancer (NSCLC) lacks specific noninvasive markers at early stage. Previous studies have indicated that several miRNAs may be potential noninvasive markers in the diagnosis of NSCLC. In the present study, we examined the expression of 9 miRNAs in serum from 128 NSCLC patients at stage I and from 79 healthy controls using quantum dot-based suspension array. Our results have demonstrated that the expression of miR-15b-5p and miR-17-5p was significantly increased in the serum of NSCLC cases, while the expression of miR-20a-5p, miR-16-5p, and miR-19a-3p were downregulated in NSCLC patients. Receiver operating characteristic (ROC) curve analysis showed that the ratios of miR-15b-5p/miR-20a-5p and miR-15b-5p/miR-16-5p have the best performance for the diagnosis of early-stage NSCLC with a specificity of 83.2% and 79.2% and sensitivity of 74.3% and 86.8%, respectively. The AUCs were 0.842 and 0.831. In summary, miR-15b-5p/miR-20a-5p and miR-15b-5p/miR-16-5p ratios were both important indicators as well as CEA and CYFRA21-1 for the diagnosis of stage I NSCLC. The ratios of miR-15b-5p/miR-20a-5p and miR-15b-5p/miR-16-5p could be used as novel noninvasive biomarkers for NSCLC diagnosis at early stage, particularly combined with serum CEA and CYFRA21-1 results.

1. Background

Non-small cell lung cancer (NSCLC) is one of the leading causes of cancer-related deaths in China or throughout the world [1]. At present, most NSCLC patients are diagnosed with advanced stages and less than 10% of them can survive more than 5 years [2], whereas the survival rate can reach up to 92% for patients with clinical stage I who undergo surgical resection within one month after diagnosis [3]. The establishment of a noninvasive and effective detection of early NSCLC would greatly improve the survival of patients with lung cancer.

Low-dose spiral computerized tomography (LDCT) scanning is the most important method for the screening and noninvasive diagnosis of lung cancer. But it is difficult to identify the benign and malignant nodules whose diameters are less than 1 cm [4]. Serum tumor markers such as carcinoembryonic antigen (CEA), cytokeratins21-1 (CYFRA21-1), neuron-specific enolase (NSE), and squamous cell carcinoma antigen (SCC) do not show high significant

Table 1: The sequence of 9 kinds of miRNA probes.

MicroRNA	DNA sequence
hsa-miR-15b-5p	Microsphere-NH3-Uni-linker-5′-CCACCTCACACTCCACTGTAAACCATGATGTGCTGCTA-3′
hsa-miR-106a-5p	Microsphere-NH3-Uni-linker-5′-CCACCTCACACTCCACCTACCTGCACTGTAAGCACTTTT-3′
hsa-miR-92a-3p	Microsphere-NH3-Uni-linker-5′-CCACCTCACACTCCACACAGGCCGGGACAAGTGCAATA-3′
hsa-miR-20a-5p	Microsphere-NH3-Uni-linker-5′-CCACCTCACACTCCACCTACCTGCACTATAAGCACTTTA-3′
hsa-miR-28-3p	Microsphere-NH3-Uni-linker-5′-CCACCTCACACTCCACTCCAGGAGCTCACAATCTAGTG-3′
hsa-miR-146b-3p	Microsphere-NH3-Uni-linker-5′-CCACCTCACACTCCACCCAGAACTGAGTCCACAGGGCA-3′
hsa-miR-17-5p	Microsphere-NH3-Uni-linker-5′-CCACCTCACACTCCACCTACCTGCACTGTAAGCACTTTG-3′
hsa-miR-19a-3p	Microsphere-NH3-Uni-linker-5′-CCACCTCACACTCCACTCAGTTTTGCATAGATTTGCACA-3′
hsa-miR-16-5p	Microsphere-NH3-Uni-linker-5′-CCACCTCACACTCCACCGCCAATATTTACGTGCTGCTA-3′

value because of low sensitivity and specificity [5]. Circulating microRNAs (miRNAs) have been recently detected in extracellular body fluids and proved themselves as promising biomarkers for a broad spectrum of diseases [6, 7]. Circulating miRNA in peripheral blood are notably stable and resist degradation despite the presence of RNase, due to being chaperoned by Ago2 or encapsuled in exosomes [8, 9]. Real-time PCR have been widely used to detect the expression of circulating miRNAs. However, it is a low-throughput technique which can only detect one kind of miRNA in a single tube. Therefore, new detection methods which can detect a set of serum miRNAs simultaneously are required.

Fluorescence microsphere-based suspension array provides a new strategy on multiplex miRNA expression in a noninvasive manner [10, 11]. Optically encoded beads or microspheres have been used as an efficient and cost-effective platform for multiplex detection of proteins or RNAs in a single tube [12, 13]. Quantum dots (QDs) are tiny light-emitting particles on the nanometer scale and are emerging as a new class of fluorescent labels for biology and medicine with exceptional resistance to photodegradation [14]. In this study, we evaluated the sensitivity and specificity of 9 circulating miRNAs and the paired miRNA ratios for the early diagnosis of NSCLC using fluorescence microsphere-based suspension array.

2. Methods

2.1. Sample Collection and Determination of Serum CEA and CYFRA21-1. All the 128 blood samples from patients diagnosed with stage I NSCLC and 79 samples from healthy donors in this study were collected from Shanghai Pulmonary Hospital. Written informed consents were obtained from all patients and volunteers before the study, and the study was approved by the ethics committee of Shanghai Pulmonary Hospital. The serum levels of tumor markers CEA and CYFRA21-1 were measured with an ELISA kit (CanAg Diagnostics, China) according to the instruction of the manufacturer.

2.2. miRNA Extraction. Total miRNA was extracted from 200 μL of serum using the miRNeasy kit (QIAGEN, USA) according to the manufacturer's instruction. Before miRNA extraction, all serum samples were thawed completely on ice followed by centrifugation once at 20,000g for 15 minutes at 4°C to remove remaining cell debris. miRNA was extracted as per the manufacturer's instruction. The concentration of miRNA was measured using the NanoDrop 1000 (NanoDrop, Wilmington, USA) and stored at −80°C.

2.3. Preparation of QD-Based DNA Nanoprobes. Core/shell CdSe/ZnSe/ZnSQDs were synthesized according to the reported paper with minor modifications [15, 16]. Briefly, CdSe nanocrystal cores were prepared using thermal decomposition at 280°C. The shells were formed by deposition of ZnSe and ZnS on CdS nanocrystals using successive ion layer adsorption and reaction (SILAR) and then were surface modified with glutathione (GSH) to provide them with hydrophiling. GSH-coated QDs were coupled with a thiol-modified DNA probe using a heterobifunctional MAL-PEG-NHS as the cross-linker. The general DNA probe combined in the DNA-QD can be suitable for a variety of target detection. Its sequence is QDot-s-s-5′-AAAAAA AAAAAAAAAAAAAAGTGGAGTGTGAGGTGG-3′. The coupling of the DNA probe was verified by AGE.

The absorption spectrum of the QD solution was measured by an ultraviolet-visible spectrophotometer (UV1750, Shimadzu, Japan); the fluorescence spectrum of the QD solution was measured by a fluorescence spectrophotometer (LS55, PerkinElmer Inc., USA). The electrophoresis characteristic of the nanoparticle was observed by agarose gel electrophoresis. A transmission electron microscope (TEM) was used to test the size and distribution of QDs (Tecnai G2 Spirit 200kV).

2.4. Fluorescence Microsphere-Based Suspension Array. Optically encoded beads or microspheres have been used as an efficient and cost-effective platform for multiplex detection of proteins or RNAs in a single tube. The encoded beads were customized from Toujing Bioengineering Corp. (Shanghai,

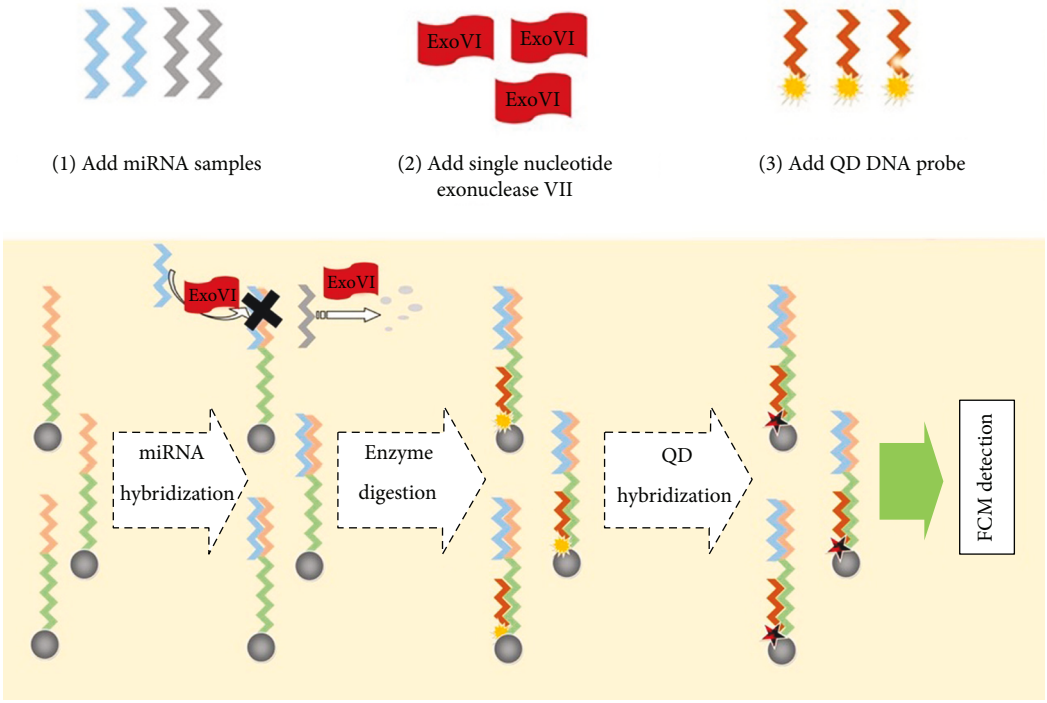

Figure 1: The diagram of the QD-based suspension arrays.

China), and the linkage of the DNA probes to beads was performed by water-soluble carbodiimide method.

Nine kinds of DNA probes for miRNA testing are synthesized and fixated on the corresponding coding microspheres to become a suspension array. The 9 probe sequences were shown in Table 1.The upper part of the DNA probes is the complementary sequence of the miRNA, and the lower segment is the complementary sequence of QD. The miRNA extraction is used to wash the microsphere. miRNAs will be combined in the upper probe of the microchip. Then the single-exonuclease automotive service engineer ExoVII is used to digest the single-strand probe without combination of miRNAs. After the hybridization and digestion, the microchip was washed and the probes without combined miRNA were removed. On the contrary, the probes with combined miRNAs were still fixated on the solid matrix. Then general DNA-QDs were hybridized to this microchip. The fluorescence intensity of QDs is proportionate to the content of fixated miRNA on the solid matrix (Figure 1).

The fluorescence intensity of QDs was measured by the flow cytometry (FCM) instrument (BD Company Accuri C6). Software Flow Joe7.6 was used to analyze the data. 300 μL of sample was performed to the FCM, and the relative fluorescence intensity of each miRNA coding beads was read as FL3 and FL4 double parameters. The FL2 was used to determine the content of each miRNA. Samples can be calculated to measure the content of miRNAs through the preset standard curve.

2.5. Statistical Analysis. Statistical comparison of the demographic features between the NSCLC cases and control samples or between the NSCLC cases was performed by using Student's t-test. The differences were considered statistically significant at $p < 0.05$. Risk score analysis was performed to evaluate the associations between NSCLC and the expression levels of the serum miRNAs. All the statistical analyses were performed with Statistical Product and Service Solutions19.0 (Spss 19.0).

3. Results

3.1. Synthesis and Characterization of QD-Based DNA Nanoprobes. The core CdSe QDs were prepared and several layers of ZnSe and ZnS shells were coated on the surface of the CdSe QDs by successive ionic layer adsorption and reaction (SILAR). Thus the oil-soluble CdSe/ZnSe/Zns core/shell QD was obtained. In order to transfer the oil-soluble QDs to water-soluble QDs, the surface of QDs was modified with functional PEG spaced by GSH. As showed in Figure 2(a), the TEM image showed the homogenous distribution of GSH-QDs with uniform size. Figure 2(b) showed that with the increased ratio of coupling reagent of NHS-PEG-Mal, the electrophoresis migration rate of GSH-QDs in the AGE was significantly decreased, which demonstrated the coupling of functional PEG with QDs increasing the particle size of QDs. The migration rate of QDs no longer changed when the ratio of QD to PEG decreased to 1 : 2000, suggesting saturated modification of PEG on the surface of QDs.

Figure 2(c) showed the AEG images of PEG-GSH-QDs coupled with DNA probe. The terminal sulfhydryl-modified DNA probe was used to couple with the PEG-GSH-QDs. The electrophoresis migration obviously increased after being coupled with DNA probe because of the negative charge of DNA, indicating successful linkage of DNA and QDs. Figure 2(d) showed the ultraviolet-visible

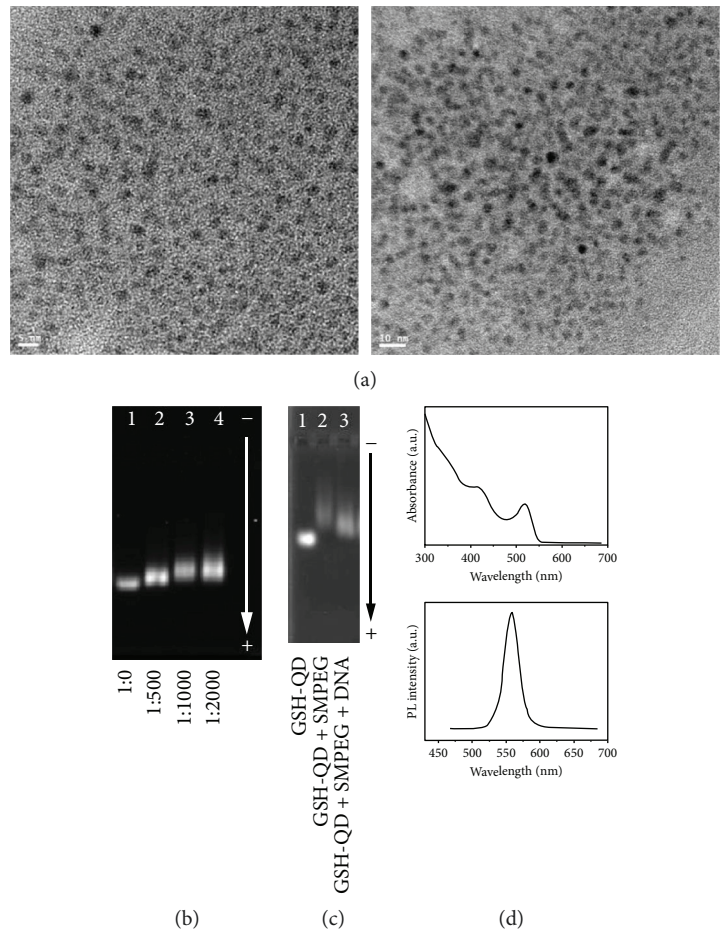

Figure 2: (a) TEM image of QDs. (b) The agarose gel electrophoresis imaging of QDs and PEG cross-linker-modified QDs. (c) The agarose gel electrophoresis imaging of QD-based DNA nanoprobes, prepared by different reaction conditions. (d) The spectroscopic properties of QD-based DNA nanoprobes. The absorbance and emission spectra were denoted by a dash line and a solid line, respectively.

absorption and emission spectrum of DNA-PEG-GSH-QDs. The emission peak was narrow and symmetric with a wavelength of around 560 nm.

3.2. miRNA Detection by Nano-QD Suspension Array. According to our circulating miRNA liquid microchip detection method based on nano-QD technology, we can simultaneously test the contents of multiple miRNAs in a single tube (Figure 3). In order to find the abnormal expression of miRNAs in NSCLC, we initially screened serum expression levels of 9 miRNAs from 207 samples, including 128 patients with NSCLC stages I and II and 79 healthy controls (Table 2). As shown in Table 3, we found that the expression of 7 miRNAs in NSCLC group has remarkable differences from that of the control group ($p < 0.05$). They are hsa-miR-92a-3p, hsa-miR-20a-5p, hsa-miR-15b-5p, hsa-miR-17-5p, hsa-miR-146b-3p, hsa-miR-16-5p, hsa-miR-19a-3, and has-miR-1. Among them, the expression of has-miR-15b-5p, has-miR-17-5p, and has-miR-146b-3p was significantly higher in NSCLC patients, while the expression of hsa-miR-92a-3p, hsa-miR-20a-5p, hsa-miR-16-5p, and hsa-miR-19a-3p was significantly lower in NSCLC patients.

3.3. Diagnostic Value Evaluation of Circulating miRNAs for NSCLC. In order to determine the values of these 9 miRNAs in diagnosis of NSCLC, we analyzed them by receiver operating characteristic (ROC) (Figure 4). The expression of hsa-miR-15b-5p and hsa-miR-17-5p was significantly increased in the serum of NSCLC cases. Under ROC curves, the area under curve (AUC) for them was 0.776 and 0.685, respectively. However, the expression of hsa-miR-20a-5p, hsa-miR-16-5p, and hsa-miR-19a-3p was downregulated in patients with NSCLC compared with the controls. The AUC for them were 0.248, 0.226, and 0.345, respectively. Based on a variety of sensitivity and misdiagnosis rates on ROC, the Youden index (YI) was used to calculate the best cut-off value of the abovementioned 5 miRNAs for early diagnosis of NSCLC. The formula is YI = sensitivity + specificity − 1. When the YI is highest, the relative level of miRNA is the best cut-off value. The results are showed as follows: the best cut-off value for hsa-miR-20a-5p is 23,059, YI is −0.515; the best cut-off value for hsa-miR-15b-5p is 4108, YI is 0.549; the best cut-off value for hsa-miR-17-5p is 11,583, YI is 0.422; the best cut-off value for hsa-miR-16-5p is 26,739, YI is −0.581; and the best cut-off value for hsa-miR-19a-3p is

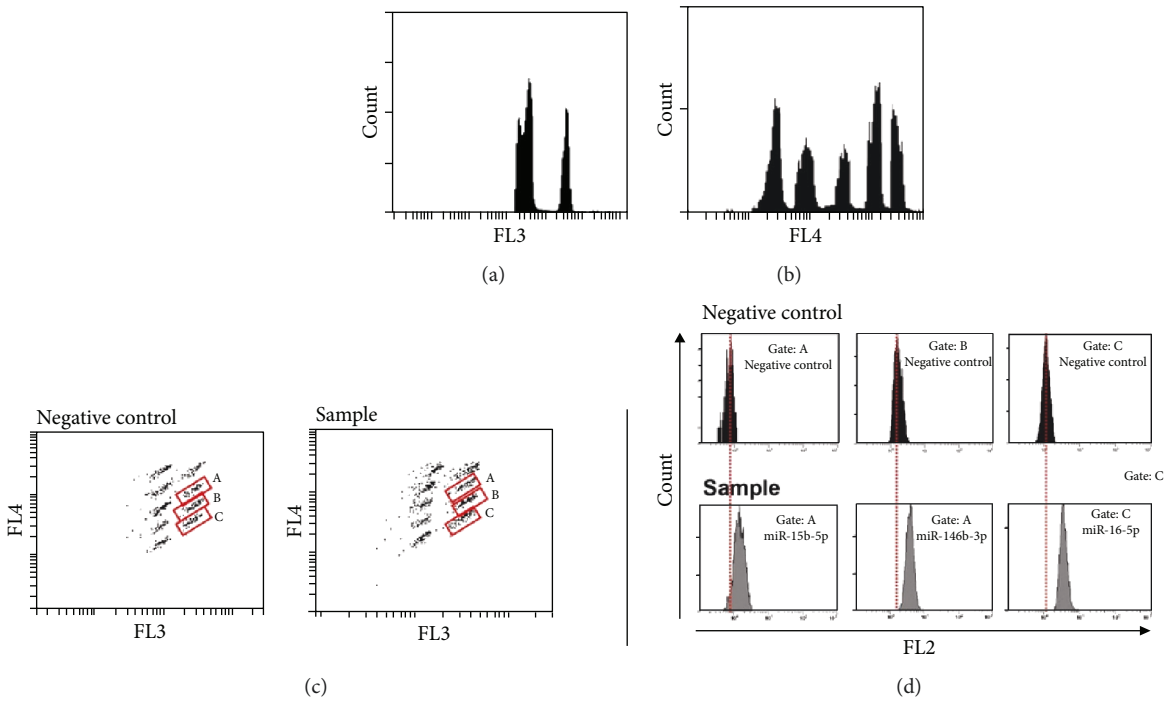

Figure 3: Flow cytometry instrument to detect fluorescent microsphere, coding, and quantum dot fluorescent signal.

Table 2: Clinical features of NSCLC patients.

Variable	Number (%)
Age (years)	
Median (IQR)	58 (49.8–67.0)
Gender	
Male	73 (57.0%)
Female	55 (43.0%)
Histological types	
Adenocarcinoma	76 (59.4%)
Squamous cell carcinoma	23 (18.0%)
Adenosquamous carcinoma	7 (5.5%)
Large cell carcinoma	5 (3.9%)
NOS (not otherwise specified)	17 (13.3%)
TNM	
Stage I	128 (100%)

22,354, YI is −0.344. We defined the values of hsa-miR-17-5p and hsa-miR-15b-5p to be higher than the best cut-off value as positive, while the values of hsa-miR-20a-5p, hsa-miR-16-5p, and hsa-miR-19a-3p are lower than the best cut-off value as positive. According to each cut-off value, the specificity and sensitivity of 5 miRNAs for diagnosis of NSCLC was calculated and compared with pathological diagnosis, which is the golden standard for NSCLC diagnosis. The sensitivity and specificity of has-miR-20a-5p, hsa-miR-15b-5p, hsa-miR-17-5p, hsa-miR16-5p, and hsa-miRN-19a-3p were 0.776 and 0.836, 0.838 and 0.695, 0.759 and 0.659, 0.797 and 0.679, and 0.723 and 0.679, respectively (Table S1). It demonstrated that these 5 circulating miRNAs have high sensitivity and specificity for early diagnosis of NSCLC, separately.

Table 3: Comparison of expression of 9 miRNAs between the NSCLC group and the healthy group.

miRNA	Group	Mean	Standard deviation	p value
hsa-miR-106a-5p	Healthy	$1.58E+06$	$9.15E+06$	0.49849
	NSCLC	$7.52E+05$	$5.93E+06$	
hsa-miR-92a-3p	Healthy	$1.83E+04$	$1.02E+04$	0.03356
	NSCLC	$1.54E+04$	$8.56E+03$	
hsa-miR-20a-5p	Healthy	$2.59E+04$	$1.31E+04$	0.001
	NSCLC	$1.64E+04$	$5.36E+03$	
hsa-miR-28-3p	Healthy	$1.45E+04$	$7.51E+03$	0.19531
	NSCLC	$2.43E+04$	$6.14E+04$	
hsa-miR-15b-5p	Healthy	$6.87E+03$	$1.06E+04$	0.04004
	NSCLC	$9.15E+05$	$3.78E+06$	
hsa-miR-17-5p	Healthy	$1.12E+04$	$8.97E+03$	0.00021
	NSCLC	$1.73E+04$	$1.17E+04$	
hsa-miR-146b-3p	Healthy	$1.17E+04$	$9.90E+03$	0.03454
	NSCLC	$2.78E+04$	$5.62E+04$	
hsa-miR-16-5p	Healthy	$3.16E+04$	$1.71E+04$	0.001
	NSCLC	$1.57E+04$	$6.50E+03$	
hsa-miR-19a-3p	Healthy	$2.41E+04$	$1.39E+04$	0.00027
	NSCLC	$1.78E+04$	$9.89E+03$	

3.4. Diagnostic Value Evaluation of Paired miRNAs for NSCLC. One important problem is that the circulating serum miRNA detection lacks a reliable inner reference, since this

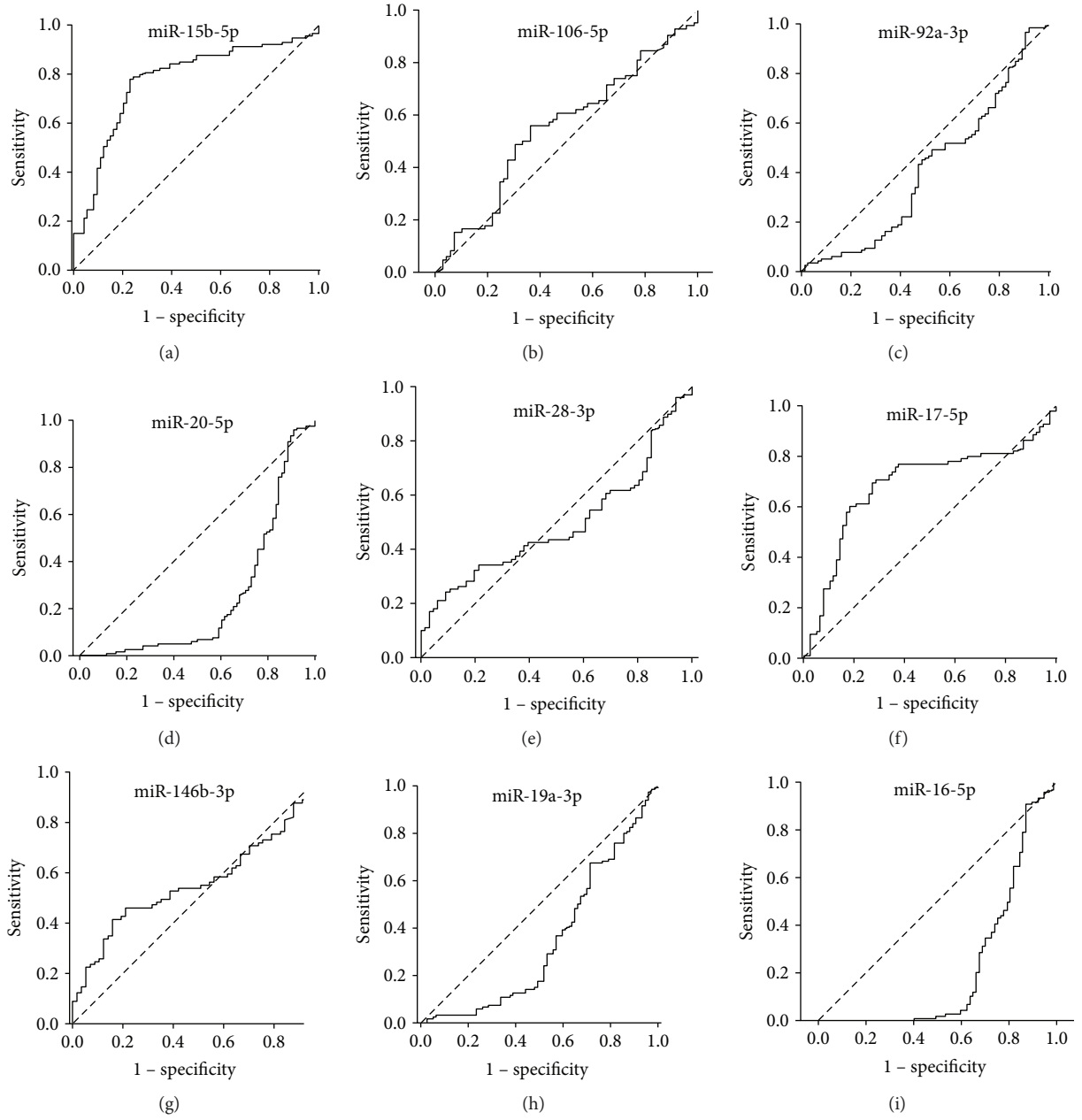

Figure 4: ROC plots of the 9 miRNAs from the test set.

liquid QD microchip hybridization method can simultaneously detect a variety of miRNAs in a single tube. However, this problem can be solved by using the paired miRNA ratio (content of lowest expressed miRNA versus content of higher expressed miRNA) to evaluate the diagnosis value for NSCLC. We analyzed the paired differentially expressed miRNA values of hsa-miR-15b-5p/hsa-miR-16-5p, hsa-miR-15b-5p/hsa-miR-20a-5p, hsa-miR-17-5p/hsa-miR-20a-5p, and hsa-miR-17-5p/hsa-miR-16-5p by ROC (Figure 5). The AUC for them were 0.831, 0.842, 0.784, and 0.808, respectively. Then we chose two miRNA pairs with higher AUC for further study. The best cut-off value for hsa-miR-15b-5p/hsa-miR-20a-5p is 0.2599 and YI is 0.577. The best cut-off value for miR-15b-5p/hsa-miR-16-5p is 0.122 and YI is 0.567. We defined the values of hsa-miR-15b-5p/hsa-miR-20a-5p and hsa-miR-15b-5p/hsa-miR-16-5p as higher than the best cut-off value as positive. According to each cut-off value, the specificity and sensitivity of these two paired miRNAs for diagnosis of NSCLC can also be calculated and compared with the golden standard (biopsy) (Table S2). The results showed that evaluation of specificity and sensitivity of NSCLC can be further improved by using paired miRNA ratio as diagnostic index. The sensitivity and specificity for diagnostic has-miR-15b-5p/hsa-miR-20a-5p and has-miR-15b-5p/hsa-miR-16-5p were 0.792 and 0.868 and 0.832 and 0.743, respectively.

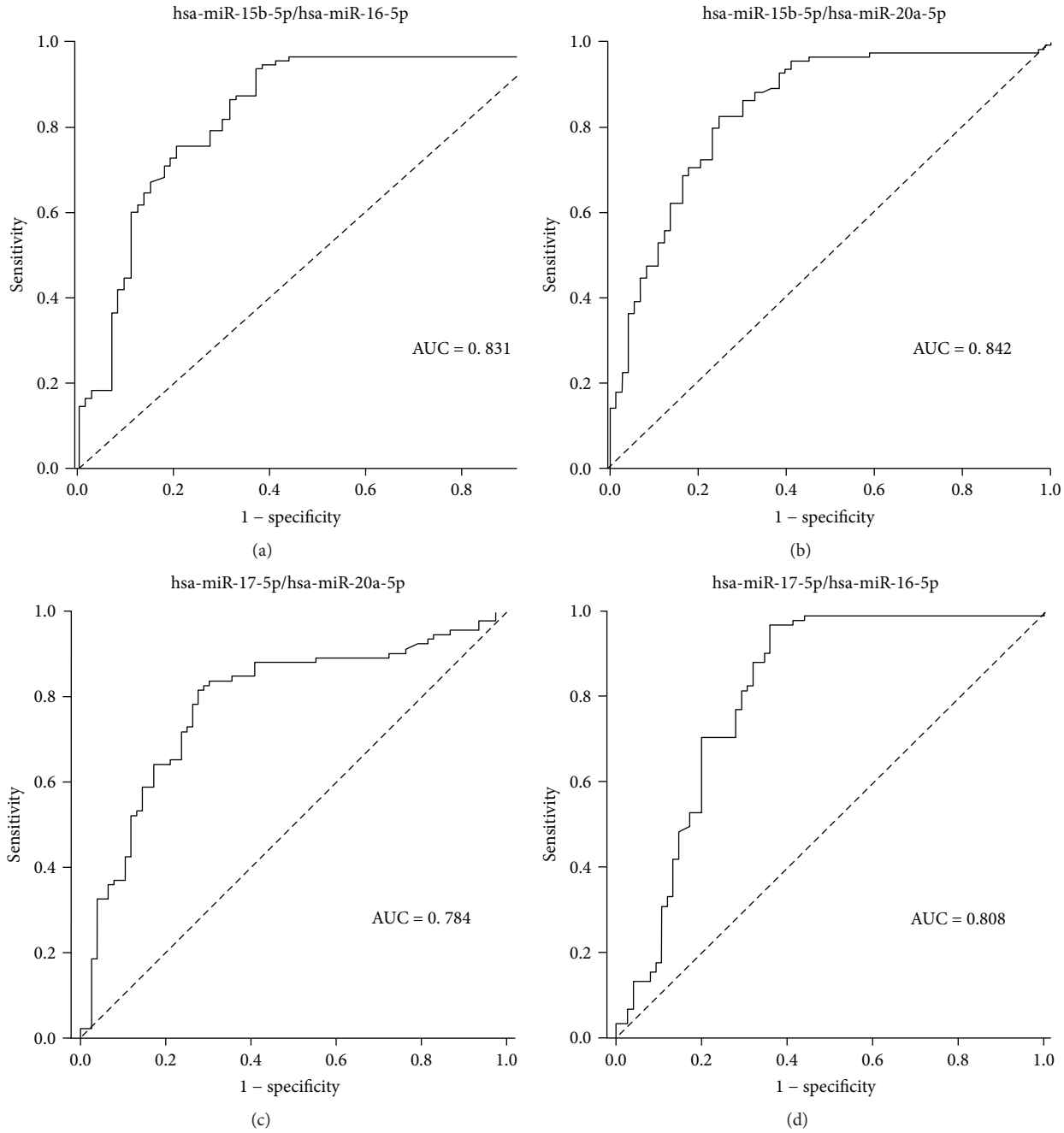

Figure 5: ROC plots of the ratio of miR-15b-5p/miR-20a-5p or miR-15b-5p/miR-16-5p from the test set.

3.5. Comparison of Paired miRNA Ratios with Serum CEA and CYFRA21-1 in Early Diagnosis of Early NSCLC. CEA and CYFRA21-1 are commonly used for the serum diagnosis of NSCLC. We compared the sensitivity and specificity of paired miRNA ratios with serum CEA and CYFRA21-1 in the 128 cases of stage I NSCLC (Figure 6). It demonstrated that serum CEA and CYFRA21-1 have little discriminatory power for diagnosis of early-stage NSCLC with AUC 0.559 and 0.508, respectively. The has-miR-15b-5p/hsa-miR-20a-5p and has-miR-15b-5p/hsa-miR-16-5p ratios were much better than those of CEA and CYFRA21-1 for the diagnosis of stage I NSCLC.

4. Discussion

Lung cancer is still the leading cause of cancer-related mortality both worldwide and in China, especially NSCLC. The main obstacle is that the diagnosis of NSCLC is usually made at advanced stages. In the recent years, researchers have found that there are a large number of stable existing miRNAs in serum, named as circulating miRNAs. The circulating miRNA can be combined with Ago2 to form Ago2-miRNA protein complex so as to escape the RNase degradation in serum. Hence, circulating miRNA as a noninvasive detection method satisfies all the requirements for the ideal tumor

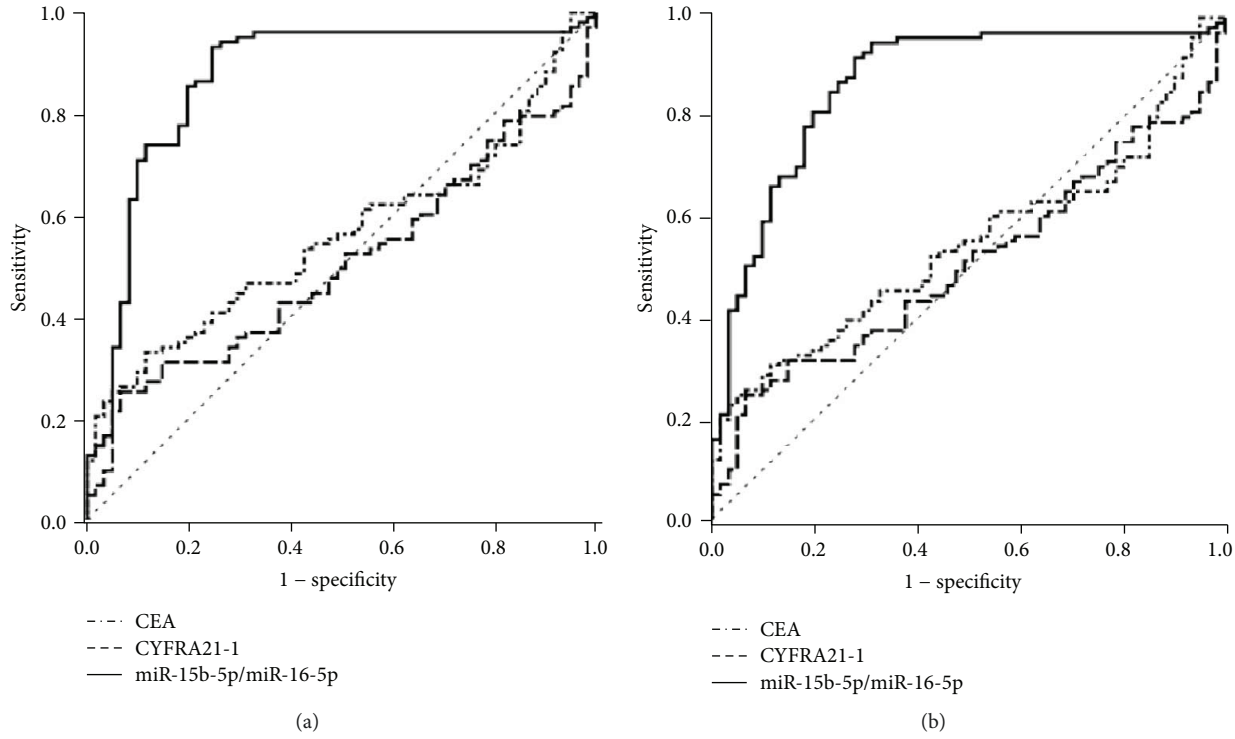

Figure 6: Comparison of the AUC of the paired miRNA ratios with CEA and CYFRA21-1.

biomarkers [17]. The detection of serum miRNAs has provided a new opportunity for early noninvasive diagnosis of NSCLC.

The quantum dot-based suspension array provides a miRNA detection method with high throughput. This serum miRNA detection method may enhance the sensitivity and specificity of diagnosis for early NSCLC. Semiconductor quantum dot can produce fluorescence by absorbing exciting light [18]. Comparing with organic fluorescent dyes, the advantages of QD include continuous excitation spectrum, narrow emission spectrum, high fluorescence efficiency, high resistance to photobleaching, and high photostability [19]. These excellent optical properties make QD a great potential in the application of immunofluorescence diagnosis, cell imaging, and living imaging and in other biological medicine areas [20]. In our study, the QD-based suspension array was able to detect low abundant miRNAs. Meanwhile, the QD with multiple shells has advantages such as high fluorescence and stable luminescence; thus, the sensitivity is greatly improved. For the high specificity, exonuclease ExoVII was used to digest nonhybrid probe, which could eliminate the influence of nonspecific adsorption on the determination results at maximum.

In the previous study, we used a high-throughput testing for the miRNA expression profile in serum and found that 15 miRNAs were upregulated in stage I and II NSCLC patients while 23 miRNAs were downregulated. Among these deregulated miRNAs, 9 miRNAs have not been reported in the literature. They are hsa-miR-92a-3p, hsa-miR-20a-5p, hsa-miR-15b-5p, hsa-miR-17-5p, hsa-miR-146b-3p, hsa-miR-16-5p, hsa-miR-19a-3p, hsa-miR-106a-5p, and hsa-miR-28-3p. So, in this study, we only selected these 9 miRNAs for further analysis and found expression of 5 miRNAs significantly increased. The higher expression of hsa-miR-15b-5p and hsa-miR-17-5p or lower expression of hsa-miR-16-5p, hsa-miR-19a-3p, and hsa-miR-20a-5p may predict the risk of NSCLC. Furthermore, we found that the ratios of two differentially expressed miRNAs such as hsa-miR-15b-5p/hsa-miR-20a-5p and hsa-miR-15b-5p/hsa-miR-16-5p were also able to discriminate NSCLC from healthy controls with better sensitivity and specificity than serum CEA and CYFRA21-1.

5. Conclusions

In conclusion, we demonstrated that the profiling of 5 serum miRNAs including hsa-miR-15b-5p, hsa-miR-20a-5p, hsa-miR-16-5p, hsa-miR-19a-3p, and hsa-miR-17-5p and the two miRNA pairs including hsa-miR-15b-5p/hsa-miR-20a-5p and hsa-miR-15b-5p/hsa-miR-16-5p could provide a novel noninvasive biomarker for NSCLC diagnosis at early stage and suggest predictable potential for clinical application.

Abbreviations

NSCLC: Non-small cell lung cancer
LDCT: Low-dose spiral computerized tomography
miRNAs: MicroRNAs
QDs: Quantum dots
SILAR: Successive ion layer adsorption and reaction
GSH: Glutathione
TEM: Transmission electron microscope

FCM: Flow cytometry
ROC: Receiver operating characteristic
AUC: Area under the curve
YI: Youden's index.

Data Availability

The datasets used and/or analyzed during the current study are available from the corresponding author on reasonable request.

Ethical Approval

The study was approved by the ethics committee of Shanghai Pulmonary Hospital.

Consent

Written informed consents were obtained from all patients and volunteers before the study.

Conflicts of Interest

The authors declare that they have no competing interests.

Authors' Contributions

Lihong Fan and Bo Su conceived the experiments. Hao Chen wrote the paper. Hao Chen and Qing Xia performed the experiments. Huiwei Qi and Changhui Wang helped to do the experiments and provided patient information. Huiwei Qi, Hao Chen, Junliang Teng, and Dan Li contributed to the analysis and revised this manuscript. Lihong Fan and Hao Chen contributed equally to this work.

Acknowledgments

This work was supported by the Foundation of Shanghai Health and Family Planning Commission (no. 20134014), Chinese National Natural Science Foundation (no. 81473469), and Fundamental Research Funds for the Central Universities (no. 20153590).

Supplementary Materials

Table S1 illustrates the chi-squared test between the diagnostic miRNAs and golden standard. Table S2 illustrates the chi-squared test between the paired miRNAs and golden standard. *(Supplementary Materials)*

References

[1] R. L. Siegel, K. D. Miller, and A. Jemal, "Cancer statistics, 2015," *CA: A Cancer Journal for Clinicians*, vol. 65, no. 1, pp. 5–29, 2015.

[2] P. Goldstraw, D. Ball, J. R. Jett et al., "Non-small-cell lung cancer," *The Lancet*, vol. 378, no. 9804, pp. 1727–1740, 2011.

[3] J. S. Donington, Y. T. Kim, B. Tong et al., "Progress in the management of early-stage non–small cell lung cancer in 2017," *Journal of Thoracic Oncology*, vol. 13, no. 6, pp. 767–778, 2018.

[4] C. D. Jeffers, T. Pandey, K. Jambhekar, and M. Meek, "Effective use of low-dose computed tomography lung cancer screening," *Current Problems in Diagnostic Radiology*, vol. 42, no. 5, pp. 220–230, 2013.

[5] S. Ma, L. Shen, N. Qian, and K. Chen, "The prognostic values of CA125, CA19.9, NSE, AND SCC for stage I NSCLC are limited," *Cancer Biomarkers*, vol. 10, no. 3-4, pp. 155–162, 2011.

[6] A. Keller, P. Leidinger, R. Gislefoss et al., "Stable serum miRNA profiles as potential tool for non-invasive lung cancer diagnosis," *RNA Biology*, vol. 8, no. 3, pp. 506–516, 2011.

[7] X. Chen, Z. Hu, W. Wang et al., "Identification of ten serum microRNAs from a genome-wide serum microRNA expression profile as novel noninvasive biomarkers for nonsmall cell lung cancer diagnosis," *International Journal of Cancer*, vol. 130, no. 7, pp. 1620–1628, 2012.

[8] S. A. Melo, et al.H. Sugimoto, J. T. O'Connell et al., *Cancer Cell*, vol. 26, no. 5, pp. 707–721, 2014.

[9] L. Li, D. Zhu, L. Huang et al., "Argonaute 2 complexes selectively protect the circulating microRNAs in cell-secreted microvesicles," *PLoS One*, vol. 7, no. 10, article e46957, 2012.

[10] D. Li, Y. Wang, C. Lau, and J. Lu, "xMAP array microspheres based stem-loop structured probes as conformational switches for multiplexing detection of miRNAs," *Analytical Chemistry*, vol. 86, no. 20, pp. 10148–10156, 2014.

[11] J. Lee, S. U. Moon, Y. S. Lee et al., "Quantum dot-based molecular beacon to monitor intracellular microRNAs," *Sensors*, vol. 15, no. 6, pp. 12872–12883, 2015.

[12] B. H. Jun, C. Rho, J. W. Byun et al., "Multilayer fluorescence optically encoded beads for protein detection," *Analytical Biochemistry*, vol. 396, no. 2, pp. 313–315, 2010.

[13] K. Sorensen, "Individualized miRNA assay panels using optically encoded beads," *Methods in Molecular Biology*, vol. 822, pp. 131–141, 2012.

[14] A. M. Smith, H. Duan, A. M. Mohs, and S. Nie, "Bioconjugated quantum dots for in vivo molecular and cellular imaging," *Advanced Drug Delivery Reviews*, vol. 60, no. 11, pp. 1226–1240, 2008.

[15] Z. A. Peng and X. Peng, "Formation of high-quality CdTe, CdSe, and CdS nanocrystals using CdO as precursor," *Journal of the American Chemical Society*, vol. 123, no. 1, pp. 183-184, 2001.

[16] J. J. Li, Y. A. Wang, W. Guo et al., "Large-scale synthesis of nearly monodisperse CdSe/CdS core/shell nanocrystals using air-stable reagents via successive ion layer adsorption and reaction," *Journal of the American Chemical Society*, vol. 125, no. 41, pp. 12567–12575, 2003.

[17] W. Z. Świtlik and J. Szemraj, "Circulating miRNAs as non-invasive biomarkers for non-small cell lung cancer diagnosis, prognosis and prediction of treatment response," *Postępy Higieny i Medycyny Doświadczalnej*, vol. 71, pp. 649–662, 2017.

[18] W. Liu, M. Howarth, A. B. Greytak et al., "Compact biocompatible quantum dots functionalized for cellular imaging," *Journal of the American Chemical Society*, vol. 130, no. 4, pp. 1274–1284, 2008.

[19] P. Zrazhevskiy, M. Sena, and X. Gao, "Designing multifunctional quantum dots for bioimaging, detection, and drug delivery," *Chemical Society Reviews*, vol. 39, no. 11, pp. 4326–4354, 2010.

[20] W. C. Chan and S. Nie, "Quantum dot bioconjugates for ultrasensitive nonisotopic detection," *Science*, vol. 281, no. 5385, pp. 2016–2018, 1998.